Composites: Part B 44 (2013) 283–294

Contents lists available at SciVerse ScienceDirect

Composites: Part B

journal homepage: www.elsevier.com/locate/compositesb

Null-field approach for the antiplane problem with elliptical holes and/or inclusions

Ying-Te Lee [a], Jeng-Tzong Chen [a,b,*]

[a] Department of Harbor and River Engineering, National Taiwan Ocean University, Keelung 20224, Taiwan
[b] Department of Mechanical and Mechatronic Engineering, National Taiwan Ocean University, Keelung 20224, Taiwan

ARTICLE INFO

Article history:
Received 4 January 2012
Received in revised form 16 April 2012
Accepted 22 May 2012
Available online 15 June 2012

Keywords:
B. Elasticity
B. Fiber/matrix bond
B. Defects
C. Numerical analysis

ABSTRACT

In this paper, we extend the successful experience of solving an infinite medium containing circular holes and/or inclusions subject to remote shears to deal with the problem containing elliptical holes and/or inclusions. Arbitrary location, different orientation, various size and any number of elliptical holes and/or inclusions can be considered. By fully employing the elliptical geometry, fundamental solutions were expanded into the degenerate kernel by using an addition theorem in terms of the elliptic coordinates and boundary densities are described by using the eigenfunction expansion. The difference between the proposed method and the conventional boundary integral equation method is that the location point can be exactly distributed on the real boundary without facing the singular integral and calculating principal value. Besides, the boundary stress can be easily calculated free of the Hadamard principal values. It is worthy of noting that the Jacobian terms exist in the degenerate kernel, boundary density and contour integral; however, these Jacobian terms would cancel each other out and the orthogonal property is preserved in the process of contour integral. This method belongs to one kind of meshless methods since only collocation points on the real boundary are required. In addition, the solution is regarded as semi-analytical form because error purely attributes to the number of truncation term of eigenfunction. An exact solution for a single elliptical inclusion is also derived by using the proposed approach and the results agree well with Smith's solutions by using the method of complex variables. Several examples are revisited to demonstrate the validity of our method.

1. Introduction

In engineering practice, saving engineering costs and how to increase the material strength are always the main concern for engineers. For this purpose, the study on stress distribution of the material containing holes or inclusions becomes an important issue. In the past, many researchers have paid attention on studying this problem. Goree and Wilson [1] used the complex-variable method and bilinear transformation to solve the problem of the infinite medium containing two circular inclusions and provided the numerical results of the normal stresses on the interface for the different radius ratio and varying spacing ratio between two inclusions. Budiansky and Carrier [2] revisited this problem by using the theory of complex variables. They derived some exact solutions for the cases of two rigid inclusions and two inclusions not rigid but touch each other. Later, Steif [3] provided the exact solution for the special case of two traction-free holes. Besides, Zimmerman [4] employed the Schwartz alternative method to discuss the stress concentration for the plane problems with two holes or inclusions and obtained a closed-form approximate solution. For a triangle pattern of three inclusions, Gong [5] employed the complex potential and Laurent series expansion to calculate the stress concentration. Based on the technique of analytical continuity and the method of successive approximation, Chao and Young [6] studied the stress concentration on a hole surrounded by two inclusions. Wu [7] solved the analytical solution for two inclusions under the remote shear in two directions by using the conformal mapping and the theorem of analytic continuation. In realistic engineering problems, however, the interface between matrix and inclusion is not always perfectly bonded. Stief [8] used the singular integral equation to solve a weakly bonded fiber composite under the longitudinal shear.

However, the use of analytical methods or complex-variable method is limited to some simple cases. The extension to the problems with multiple circular holes or inclusions may encounter difficulty. More and more researchers have paid attentions on numerical solutions. Sendeckyj [9] proposed a successive approximation method to resolve the problems containing multiple inclusions. However, the approach is more complicated and it needs a large number of truncated terms when the number of inclusions increases. Honein et al. [10] employed the Möbius transformations

* Corresponding author at: Department of Harbor and River Engineering, National Taiwan Ocean University, Keelung 20224, Taiwan. Tel.: +886 2 24622192x6177; fax: +886 2 24632375.
E-mail address: jtchen@mail.ntou.edu.tw (J.-T. Chen).

1359-8368/$ - see front matter © 2012 Elsevier Ltd. All rights reserved.
http://dx.doi.org/10.1016/j.compositesb.2012.05.025

involving the complex potential to solve the problems with two unequal holes and/or inclusions. Not only antiplane shears but also screw dislocations were considered in their works. For screw dislocation, Chen et al. [11] have solved it by using the null-field integral equation. In addition, the complex variable boundary element method (CVBEM) was also used to solve the antiplane problem with two holes under remote shear by Chou [12]. To develop a general solution for solving an infinite medium containing multiple circular inclusions with any number, radii, shear moduli and location is not trivial. Mogilevskaya and Crouch [13] utilized the Fourier series expansion in conjunction with the Galerkin method to solve the problem of circular inclusions in 2-D elasticity. Besides, Chen and his group [14] used the null-field boundary integral equation in companion with the degenerate kernels and Fourier series to solve the antiplane problem with multiple circular holes. Later, they [15,16] also extend the approach to deal with the problem containing multiple inclusions and piezoelectricity problems with arbitrary circular inclusions. The approach belongs to one kind of meshless methods and has high accuracy and exponential convergence.

The aforementioned works were limited on the circular geometric shape. For elliptical shape, it may be more general than circular geometry in the practical applications. As a result, study on the problems including elliptical geometry is interesting and important. Based on the concept of complex potential, Gong and Meguid [17] used the conformal mapping and Laurent series expansion to solve an infinite medium containing an elliptical inhomogeneity under antiplane shear. Explicit form of the stress function in the inhomogeneity as well in the matrix was derived in their work. Then, a generalized and unified treatment was developed by Gong [18] for the elliptical inclusion embedded in an infinite matrix not only under the remote shear but also interacting by screw dislocation. A similar work was implemented by Ru and Schiavone [19]. In their work, they can confirm that stress is uniform in the elliptical inclusion. Besides, Shen et al. [20] develop a semi-analytical solution for the problem of an elliptical inclusion not perfectly bonded in an infinite matrix under antiplane shear. Under the assumption of continuous tractions and discontinuous displacements across the interface, they used a model of a spring layer with thickness to simulate the interface. They found the non-uniform stress field and the average stresses in the inclusion is highly related to the aspect ratio of the inclusion and the parameter of interface simulation. However, these researches only concentrated on single elliptical inclusion. For arbitrary distributed elliptical inclusions under remote shear, Noda and Matsuo [21] have used the Cauchy-type singular integral equations to solve an interaction problem of elliptical inclusions disturbed in an infinite medium under a longitudinal shear loading. They discussed different outlet of two elliptical inclusions as well as different ratios of shear moduli. Later, Lee and Kim [22] also revisited the problem of Noda and Matsuo by using the volume integral equation method. Besides, many works were done for the plane elasticity [23–25] with multiple elliptical inclusions as well as antiplane problems. However, for antiplane elasticity with more than two elliptical inclusions, few works were found to our knowledge except [21,22]. Recently, Kuo [26] used the mulipole expansion approach in companion with a construction of consistency conditions and translation operators to deal with a number of arbitrarily dispersed elliptic cylinders bonded in an infinite isotropic matrix subject to a remote potential field. Mathematically speaking, the mathematical model of the problem solved by Kuo and the antiplane problem subject to remote shear is the same. In this paper, we present our approach to revisit the antiplane problem containing multiple elliptical inclusions.

In this paper, we extend the successful experience of solving antiplane shear for circular holes and/or inclusions to deal with the problem containing elliptical holes and/or inclusions. A problem of arbitrary location, different orientation, various size and any number of elliptical holes and/or inclusions imbedded in an isotropic and infinite medium is considered. By fully employing the elliptical geometry, fundamental solutions were expanded into the degenerate kernel by using an addition theorem in terms of the elliptical coordinates, and boundary densities are approximated by the eigenfunction expansion. In the present approach, the collocation point can be exactly located on the real boundary without calculating Cauchy principal value or Hadamard principal value. Besides, the Jacobian terms may exist in the degenerate kernel, boundary density and contour integral. Nevertheless, these Jacobian terms would cancel each other out and the orthogonal property is preserved in contour integral. The proposed approach can be seen as one kind of meshless and semi-analytical methods because only collocation points on the real boundary are required and the error purely attributes to the number of truncation term of eigenfunction. An exact solution for a single elliptical inclusion is also derived by using the proposed approach. Although the representation is different from Smith's form [27], both the two solutions match well with each other in numerical implementation. Finally, several examples are revisited to demonstrate the validity of our method.

2. Problem statement

For the antiplane problem as shown in Fig. 1, the displacement field is

$$u = v = 0, \quad w = w(x,y), \tag{1}$$

where w is the only nonvanishing component of displacement and it is a function of x and y in the Cartesian coordinates. Based on the theory of elasticity, the stress components of the isotropic and elastic body are

$$\tau_{xz} = \tau_{zx} = \mu \frac{\partial w}{\partial x}, \tag{2}$$

$$\tau_{yz} = \tau_{zy} = \mu \frac{\partial w}{\partial y}, \tag{3}$$

where μ is the shear modulus. The equilibrium equation in elasticity can be simplified to

$$\frac{\partial \tau_{xz}}{\partial x} + \frac{\partial \tau_{yz}}{\partial y} = 0. \tag{4}$$

Therefore, we have

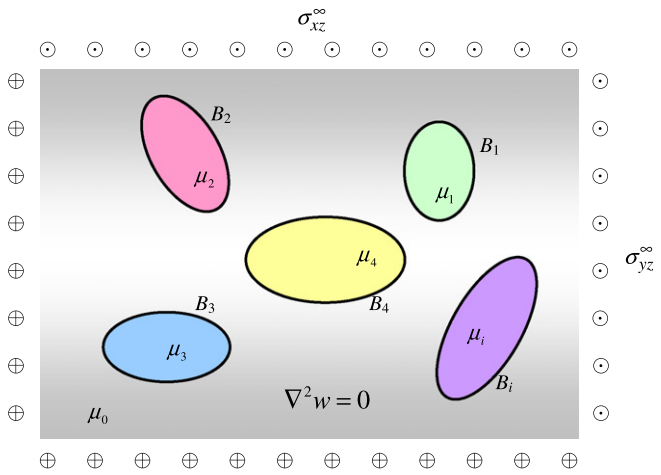

Fig. 1. Sketch of the problem containing multiple elliptical inclusions under remote shears.

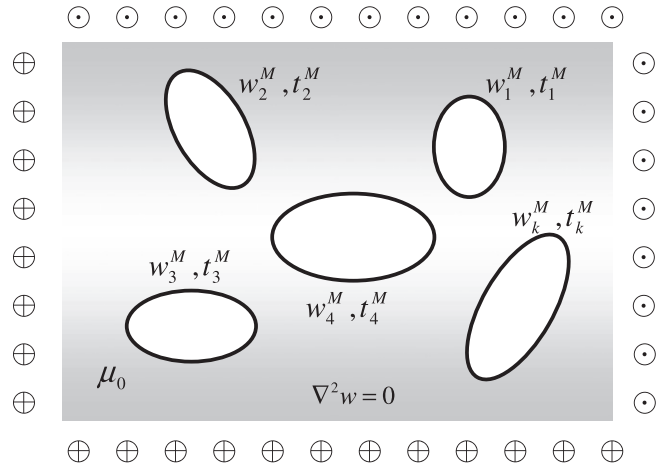

Fig. 2a. An infinite plane with multiple holes under the remote shears.

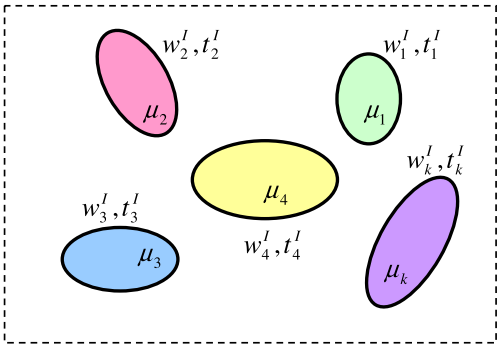

Fig. 2b. Each isolated inclusion.

$$\frac{\partial^2 w}{\partial x^2} + \frac{\partial^2 w}{\partial y^2} = \nabla^2 w = 0. \tag{5}$$

As shown in Eq. (5), the antiplane problem is governed by the Laplace equation. Here, an antiplane problem with N elliptical inclusions subject to remote shears is considered as shown in Fig. 1. By taking free body technique with respect to each inclusion, the problem in Fig. 1 is decomposed into Figs. 2a and 2b. One is an infinite plane with multiple elliptical holes under remote shears and the other is the problem of multiple isolated inclusions where each individual inclusion is governed by the Laplace equation. In the interface between the matrix and inclusion, the continuity of displacement and equilibrium of traction are given as follows:

$$w_k^M = w_k^I, \tag{6}$$
$$\mu_0 t_k^M + \mu_k t_k^I = 0, \tag{7}$$

where the subscripts of M and I denote matrix and inclusion, respectively, μ_0 and μ_k denote the shear moduli of matrix and the kth inclusion, respectively, and t_k^M and t_k^I are the tractions of matrix and inclusion, respectively. The problem in Fig. 2a can be further decomposed as shown in Figs. 3a and 3b. In Fig. 3a, the matrix is homogenous and isotropic, and bears the uniform shear stresses, τ_{xz}^∞ and τ_{yz}^∞, at infinity or equivalently disturbs by the displacement

$$w^\infty = \frac{\tau_{xz}^\infty}{\mu_0} x + \frac{\tau_{yz}^\infty}{\mu_0} y. \tag{8}$$

The two problems in Figs. 2b and 3b can be solved by using the present approach as mentioned in the next section.

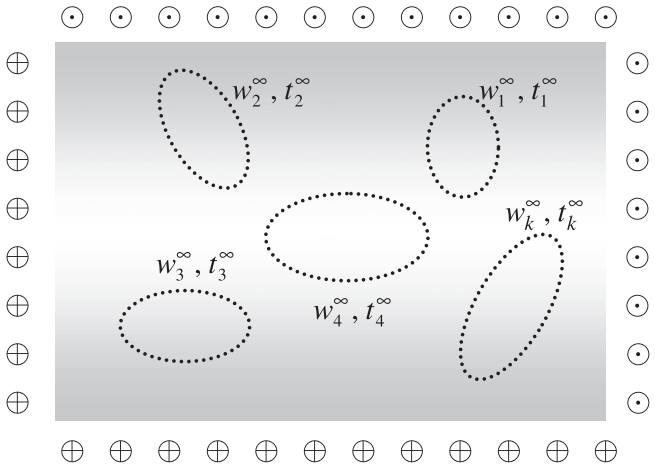

Fig. 3a. An infinite plane with remote shears.

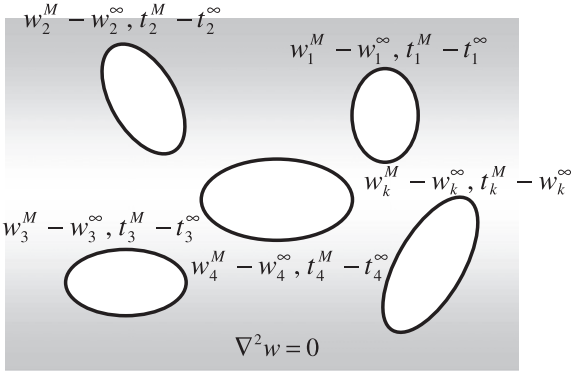

Fig. 3b. A problem of an infinite plane containing multiple holes.

3. Dual null-field integral formulation

3.1. Dual null-field integral equations – the conventional version

The integral equation for the domain point can be derived from the third Green's identity, we have

$$w(\mathbf{x}) = \int_B T(\mathbf{s},\mathbf{x}) w(\mathbf{s}) dB(\mathbf{s}) - \int_B U(\mathbf{s},\mathbf{x}) t(\mathbf{s}) dB(\mathbf{s}), \quad \mathbf{x} \in D, \tag{9}$$
$$t(\mathbf{x}) = \int_B M(\mathbf{s},\mathbf{x}) w(\mathbf{s}) dB(\mathbf{s}) - \int_B L(\mathbf{s},\mathbf{x}) t(\mathbf{s}) dB(\mathbf{s}), \quad \mathbf{x} \in D, \tag{10}$$

where $\mathbf{s}$ and $\mathbf{x}$ are the source and field points, respectively, $t(\mathbf{x}) = \frac{\partial u(\mathbf{x})}{\partial \mathbf{n}_\mathbf{x}}$, $t(\mathbf{s}) = \frac{\partial w(\mathbf{s})}{\partial \mathbf{n}_\mathbf{s}}$, $\mathbf{n}_s$ and $\mathbf{n}_x$ denote the outward normal vectors at the source point $\mathbf{s}$ and field point $\mathbf{x}$, respectively, D is the domain of interest and the kernel function, $U(\mathbf{s},\mathbf{x}) = \frac{1}{2\pi} \ln r$ ($r \equiv |\mathbf{x} - \mathbf{s}|$), is the fundamental solution which satisfies

$$\nabla^2 U(\mathbf{x},\mathbf{s}) = \delta(\mathbf{x} - \mathbf{s}), \tag{11}$$

in which $\delta(\mathbf{x} - \mathbf{s})$ denotes the Dirac-delta function. The other kernel functions, $T(\mathbf{s},\mathbf{x})$, $L(\mathbf{s},\mathbf{x})$, and $M(\mathbf{s},\mathbf{x})$, are defined by

$$T(\mathbf{s},\mathbf{x}) = \frac{\partial U(\mathbf{s},\mathbf{x})}{\partial \mathbf{n}_\mathbf{s}},$$
$$L(\mathbf{s},\mathbf{x}) = \frac{\partial U(\mathbf{s},\mathbf{x})}{\partial \mathbf{n}_\mathbf{x}}, \tag{12}$$
$$M(\mathbf{s},\mathbf{x}) = \frac{\partial^2 U(\mathbf{s},\mathbf{x})}{\partial \mathbf{n}_\mathbf{s} \partial \mathbf{n}_\mathbf{x}}.$$

By moving the field point $\mathbf{x}$ to the boundary, the dual boundary integral equations for the boundary point can be obtained as follows:

$$\frac{1}{2}w(\mathbf{x}) = \text{C.P.V.}\int_B T(\mathbf{s},\mathbf{x})w(\mathbf{s})dB(\mathbf{s}) - \text{R.P.V.}\int_B U(\mathbf{s},\mathbf{x})t(\mathbf{s})dB(\mathbf{s}), \quad \mathbf{x}\in B, \tag{13}$$

$$\frac{1}{2}t(\mathbf{x}) = \text{H.P.V.}\int_B M(\mathbf{s},\mathbf{x})w(\mathbf{s})dB(\mathbf{s}) - \text{C.P.V.}\int_B L(\mathbf{s},\mathbf{x})t(\mathbf{s})dB(\mathbf{s}), \quad \mathbf{x}\in B, \tag{14}$$

where B is the boundary, R.P.V., C.P.V. and H.P.V. denote the Riemann principal value (Riemann sum), Cauchy principal value and Hadamard (or called Mangler) principal value, respectively. In the singular or hypersingular integral for either smooth or unsmooth boundary, it should be interpreted by using the sense of principal value if a technique of small circular bump is considered. For the smooth boundary, the boundary density or boundary contour integral can improve the singularity order in integration and Riemann integrals can be interpreted. To be consistent with the BEM literature [28–30], C.P.V. is employed if a small circular bump is used in the BEM formulation. The more general contours of Lipschitz type (which may include edges and corners) are mentioned in the textbooks. Here, we consider the smooth contours of circular and elliptical boundaries. No singular integrals are involved in BIE formulation if the Lipschitz condition is considered. Besides, once the field point $\mathbf{x}$ locates outside the domain ($\mathbf{x}\in\Omega$), we obtain the dual null-field integral equations as shown below

$$0 = \int_B T(\mathbf{s},\mathbf{x})w(\mathbf{s})dB(\mathbf{s}) - \int_B U(\mathbf{s},\mathbf{x})t(\mathbf{s})dB(\mathbf{s}), \quad \mathbf{x}\in D^c, \tag{15}$$

$$0 = \int_B M(\mathbf{s},\mathbf{x})w(\mathbf{s})dB(\mathbf{s}) - \int_B L(\mathbf{s},\mathbf{x})t(\mathbf{s})dB(\mathbf{s}), \quad \mathbf{x}\in D^c, \tag{16}$$

where D^c is the complementary domain. Eqs. (9), (10), (15), and (16) are conventional formulations where the point cannot be located on the real boundary. Singularity occurs and concept of principal values is required once Eqs. (13) and (14) are considered. The traction $t(\mathbf{s})$ is the directional derivative of $w(\mathbf{s})$ along the outer normal direction at $\mathbf{s}$. In order to satisfy the interface condition, the collocation points are located on the boundary. For calculating the stress in the domain, the normal vector of an interior point is artificially given, e.g. $t(\mathbf{x}) = \partial u(\mathbf{x})/\partial x_1$, if $\mathbf{n} = (1, 0)$ and $t(\mathbf{x}) = \partial u(\mathbf{x})/\partial x_2$, if $\mathbf{n} = (0, 1)$. In other words, the selection of $\vec{n}$ depends on the stress under consideration. Here, we briefly introduce the theory of integral equations. More information on the potential theory can be found in [31,32].

3.2. Dual null-field integral formulation – the present version

By introducing the degenerate kernels, the collocation point can be located on the real boundary free of calculating principal value using a small circular bump. Therefore, the representations of integral equations including the boundary point for the interior problem can be written as

$$w(\mathbf{x}) = \int_B T^i(\mathbf{s},\mathbf{x})w(\mathbf{s})dB(\mathbf{s}) - \int_B U^i(\mathbf{s},\mathbf{x})t(\mathbf{s})dB(\mathbf{s}), \quad \mathbf{x}\in D\cup B, \tag{17}$$

$$t(\mathbf{x}) = \int_B M^i(\mathbf{s},\mathbf{x})w(\mathbf{s})dB(\mathbf{s}) - \int_B L^i(\mathbf{s},\mathbf{x})t(\mathbf{s})dB(\mathbf{s}), \quad \mathbf{x}\in D\cup B, \tag{18}$$

and

$$0 = \int_B T^e(\mathbf{s},\mathbf{x})w(\mathbf{s})dB(\mathbf{s}) - \int_B U^e(\mathbf{s},\mathbf{x})t(\mathbf{s})dB(\mathbf{s}), \quad \mathbf{x}\in D^c\cup B, \tag{19}$$

$$0 = \int_B M^e(\mathbf{s},\mathbf{x})w(\mathbf{s})dB(\mathbf{s}) - \int_B L^e(\mathbf{s},\mathbf{x})t(\mathbf{s})dB(\mathbf{s}), \quad \mathbf{x}\in D^c\cup B, \tag{20}$$

once the kernels are expressed in terms of an appropriate degenerate forms (denoted by subscripts i and e) instead of the closed-form fundamental solution. It is noted that $\mathbf{x}$ in Eqs. (17)–(20) can be exactly located on the real boundary.

For the exterior problem, the domain of interest (D) is in the external region of the elliptical boundary and the complementary domain (D^c) is in the internal region of the ellipse. Therefore, the null-field integral equations are represented as

$$w(\mathbf{x}) = \int_B T^e(\mathbf{s},\mathbf{x})w(\mathbf{s})dB(\mathbf{s}) - \int_B U^e(\mathbf{s},\mathbf{x})t(\mathbf{s})dB(\mathbf{s}), \quad \mathbf{x}\in D\cup B, \tag{21}$$

$$t(\mathbf{x}) = \int_B M^e(\mathbf{s},\mathbf{x})w(\mathbf{s})dB(\mathbf{s}) - \int_B L^e(\mathbf{s},\mathbf{x})t(\mathbf{s})dB(\mathbf{s}), \quad \mathbf{x}\in D\cup B, \tag{22}$$

and

$$0 = \int_B T^i(\mathbf{s},\mathbf{x})w(\mathbf{s})dB(\mathbf{s}) - \int_B U^i(\mathbf{s},\mathbf{x})t(\mathbf{s})dB(\mathbf{s}), \quad \mathbf{x}\in D^c\cup B, \tag{23}$$

$$0 = \int_B M^i(\mathbf{s},\mathbf{x})w(\mathbf{s})dB(\mathbf{s}) - \int_B L^i(\mathbf{s},\mathbf{x})t(\mathbf{s})dB(\mathbf{s}), \quad \mathbf{x}\in D^c\cup B. \tag{24}$$

Also, $\mathbf{x}$ in Eqs. (21)–(24) can be exactly located on the real boundary. For various problems (interior or exterior), we used different kernel functions (denoted by superscripts "i" and "e") so that jump behavior across the boundary can be captured. Therefore, different expressions of the kernels for the interior and exterior observer points are used and they will be elaborated on later.

3.3. Expansions of fundamental solution and boundary density

The keypoint of derivation of the degenerate kernel is the use of addition theorem. In mathematics, the definition of an addition theorem is given below:

$$f_a(x+y) = \sum_m p_m(x)q_m(y). \tag{25}$$

The simplest addition theorem is the exponential function as shown below:

$$e^{x+y} = e^x\cdot e^y. \tag{26}$$

However, the fundamental solution needs the subtraction theorem due to

$$U(|x-y|) = \sum_m r_m(x)s_m(y). \tag{27}$$

By changing y to $-y$, the addition theorem can be extended to the subtraction theorem for the fundamental solution. In other words, the addition theorem is the re-expansion formula that allow for analytical representation of the fields written in the co-ordinate system of one ellipse in terms of the co-ordinate system of another one. The degenerate kernel used in the present work is an addition theorem for expanding the fundamental solution. Then, we used another co-ordinate system to describe the position of source point $s = (\bar{\xi}_1, \bar{\eta}_1)$ and field point $x = (\xi_1, \eta_1)$. We can have another observer for $x = (\xi_2, \eta_2)$ and $s = (\bar{\xi}_2, \bar{\eta}_2)$ to express the fundamental solution with objectivity. A figure is given in Fig. 4 for clarity.

Based on the separable property, the kernel function $U(\mathbf{s}, \mathbf{x})$ can be expanded into degenerate form by employing the separating technique for source point and field point under the elliptical coordinates. The fundamental solution, $U(\mathbf{s}, \mathbf{x})$, in terms of degenerate (separable) kernel is shown below:

$$U(\mathbf{s},\mathbf{x}) = \begin{cases} U^i(\bar{\xi},\bar{\eta};\xi,\eta) = \frac{1}{2\pi}\left(\bar{\xi} + \ln\frac{c}{2} - \sum_{m=1}^{\infty}\frac{2}{m}e^{-m\bar{\xi}}\cosh m\xi\cos m\eta\cos m\bar{\eta} - \sum_{m=1}^{\infty}\frac{2}{m}e^{-m\bar{\xi}}\sinh m\xi\sin m\eta\sin m\bar{\eta}\right), & \bar{\xi} \geqslant \xi, \\ U^e(\bar{\xi},\bar{\eta};\xi,\eta) = \frac{1}{2\pi}\left(\xi + \ln\frac{c}{2} - \sum_{m=1}^{\infty}\frac{2}{m}e^{-m\xi}\cosh m\bar{\xi}\cos m\eta\cos m\bar{\eta} - \sum_{m=1}^{\infty}\frac{2}{m}e^{-m\xi}\sinh m\bar{\xi}\sin m\eta\sin m\bar{\eta}\right), & \bar{\xi} < \xi, \end{cases} \tag{28}$$

where the position of the source point is $s = (\bar{\xi},\bar{\eta})$ and the field point is $x = (\xi,\eta)$, the superscripts "i" and "e" denote the interior ($\bar{\xi} \geqslant \xi$) and exterior ($\bar{\xi} < \xi$) cases, respectively. Fig. 5 shows the contour plot by using Eq. (28). The other kernels in the boundary integral equation can be obtained by utilizing the operators of Eq. (12) with respect to the kernel $U(\mathbf{s}, \mathbf{x})$. In the computation, the degenerate kernel can be expressed as finite sums of products of functions of $\mathbf{s}$ alone and functions of $\mathbf{x}$ alone.

Since the closed-form fundamental solution ($\ln r$) is used in the conventional BEM, the principal values of singular and hypersingular integrals have to be encountered and need to be calculated by using the small circular bump technique and the C.P.V. and H.P.V. concept. Therefore, we can obtain the jump term and derive the boundary integral equation not only from the null-field integral equation but also from the integral equation for the domain point. However, in the present formulation, we use the null-field integral equation or integral equation for the domain point in conjunction with appropriate degenerate kernel. By using the collocation method, we can easily construct a linear algebraic system. It is noted that the null-field point or the domain point can be exactly located on the real boundary when the appropriate degenerate kernels are employed. The main advantage of present formulation is that the collocation point $\mathbf{x}$ is located on the real boundary free of facing principal value using the small circular bump, while the conventional BEM needs to deal with singularities by using the upper bump or lower bump since a closed-form kernel is used. Therefore, the main difference between our approach and the conventional method is that the integral path is along the real boundary without bump to obtain the free term. Furthermore, the jump behavior for potentials of integral equations between the domain point and the null-field point is captured when various degenerate kernels for fundamental solutions are employed for the domain point and complementary domain point. In other words, the jump behavior is revealed by using various degenerate kernels for the fundamental solution instead of employing the small circular bump approach in the conventional boundary integral equation method since the jump term can be easily captured by the Wronskian. Although we construct the same linear algebraic equation, the derivation process is different. In other words, the conventional BEM is direct to capture the discontinuous function of double-layer potential using the small circular bump and principal value senses. In the present work, we used the degenerate kernel to separately describe the interior and exterior fields to capture the jump potential across boundary. By using the different integral representations in companion with appropriate degenerate kernels, we can derive a linear algebraic equation without facing singular and hypersingular integrals by collocating the observation point exactly on the boundary. Briefly speaking, the discontinuity across the boundary can be described either by C.P.V. with the small circular bump technique or by the degenerate kernel.

For the kth boundary densities, we apply the Fourier series expansions to approximate the potential $w(\mathbf{s})$ and its normal derivative $t(\mathbf{s})$ on the boundary

$$w(\mathbf{s}) = a_0 + \sum_{n=1}^{\infty} a_n \cos n\bar{\eta} + \sum_{n=1}^{\infty} b_n \sin n\bar{\eta}, \tag{29}$$

$$t(\mathbf{s}) = \frac{1}{J_s}\left(p_0 + \sum_{n=1}^{\infty} p_n \cos n\bar{\eta} + \sum_{n=1}^{\infty} q_n \sin n\bar{\eta}\right), \tag{30}$$

where a_0, a_n, b_n, p_0, p_n and q_n are the coefficients of the Fourier series, $\bar{\eta}$ is the angle ($0 \leqslant \bar{\eta} < 2\pi$) and J_s is the Jocobian with respect to the source point and the definition is

$$J_s(\bar{\xi},\bar{\eta}) = c\sqrt{(\sinh\bar{\xi}\cos\bar{\eta})^2 + (\cosh\bar{\xi}\sin\bar{\eta})^2}. \tag{31}$$

Here, it can be observed that the terms of J_s which may exist in the degenerate kernel, boundary density and boundary integral are

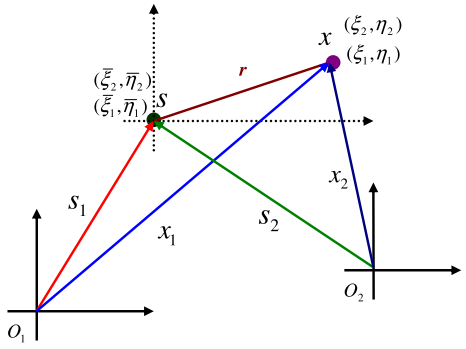

Fig. 4. Objective of the fundamental solution of different observers by using the addition theorem (separable kernel).

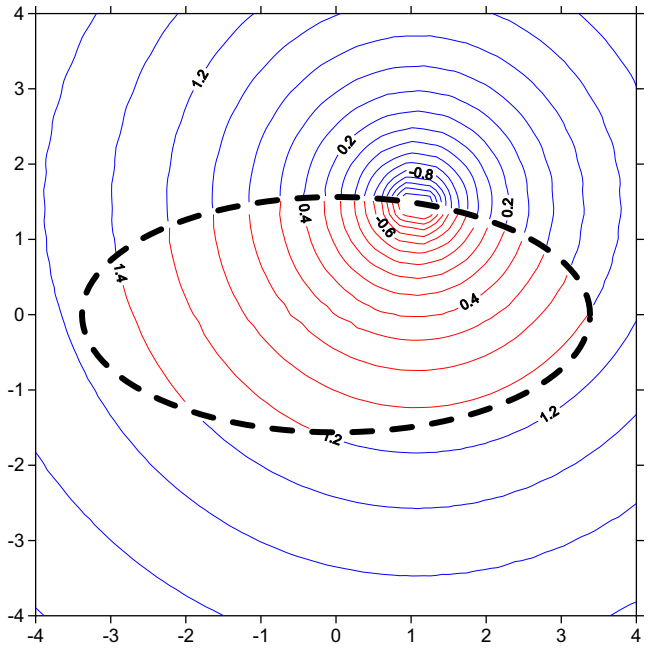

Fig. 5. Contour plot of the degenerate kernel in the elliptic coordinates to represent the closed-form fundamental solution $\ln r$.

cancelled out each other naturally in the boundary integration. Therefore, the elliptic integral is not required to deal with. In the real computation, only the finite M number of terms is used in the summation. The present method belongs to one kind of semi-analytical methods since error only attributes to the truncation of Fourier series.

3.4. Linear algebraic system

In order to calculate the Fourier coefficients, Np ($Np = 2M + 1$) boundary nodes for each elliptical boundary are needed and they are uniformly collocated on each elliptical boundary. After locating the null-field point $\mathbf{x}_k$ exactly on the kth elliptical boundary in Eq. (19) or Eq. (20), we have

$$0 = \sum_{j=1}^{N} \int_{B_j} T(\mathbf{s},\mathbf{x}) w(\mathbf{s}) dB_j(\mathbf{s}) - \sum_{j=1}^{N} \int_{B_j} U(\mathbf{s},\mathbf{x}) t(\mathbf{s}) dB_j(\mathbf{s}), \quad \mathbf{x} \in D^c \cup B, \tag{32}$$

or

$$0 = \sum_{j=1}^{N} \int_{B_j} M(\mathbf{s},\mathbf{x}) w(\mathbf{s}) dB_j(\mathbf{s}) - \sum_{j=1}^{N} \int_{B_j} L(\mathbf{s},\mathbf{x}) t(\mathbf{s}) dB_j(\mathbf{s}), \quad \mathbf{x} \in D^c \cup B. \tag{33}$$

Since the boundary integral equations are frame indifferent, i.e. objectivity rule is satisfied. The origin of observer system is adaptively chosen at the center of elliptical boundary under integration. For the B integral of the elliptical boundary, the kernels of $U(\mathbf{s},\mathbf{x})$ and $T(\mathbf{s},\mathbf{x})$ are expressed in terms of degenerate kernels, and $w(\mathbf{s})$ and $t(\mathbf{s})$ are substituted by using the Fourier series. For simplicity, a linear algebraic system is obtained

$$[\mathbf{U}]\{\mathbf{t}\} = [\mathbf{T}]\{\mathbf{w}\}, \tag{34}$$

or

$$[\mathbf{L}]\{\mathbf{t}\} = [\mathbf{M}]\{\mathbf{w}\}, \tag{35}$$

where $[\mathbf{U}]$, $[\mathbf{T}]$, $[\mathbf{L}]$ and $[\mathbf{M}]$ are the influence matrices with a dimension of $N \times (2M + 1)$ by $N \times (2M + 1)$, $\{\mathbf{u}\}$ and $\{\mathbf{t}\}$ denote the column vectors of Fourier coefficients with a dimension of $N \times (2M + 1)$ by 1 in which $[\mathbf{U}]$, $[\mathbf{T}]$, $[\mathbf{L}]$, $[\mathbf{M}]$ $\{\mathbf{u}\}$ and $\{\mathbf{t}\}$ can be defined as follows:

$$[\mathbf{U}] = \begin{bmatrix} \mathbf{U}_{11} & \mathbf{U}_{12} & \cdots & \mathbf{U}_{1N} \\ \mathbf{U}_{21} & \mathbf{U}_{22} & \cdots & \mathbf{U}_{2N} \\ \vdots & \vdots & \ddots & \vdots \\ \mathbf{U}_{N1} & \mathbf{U}_{N2} & \cdots & \mathbf{U}_{NN} \end{bmatrix}, \tag{36}$$

$$[\mathbf{T}] = \begin{bmatrix} \mathbf{T}_{11} & \mathbf{T}_{12} & \cdots & \mathbf{T}_{1N} \\ \mathbf{T}_{21} & \mathbf{T}_{22} & \cdots & \mathbf{T}_{2N} \\ \vdots & \vdots & \ddots & \vdots \\ \mathbf{T}_{N1} & \mathbf{T}_{N2} & \cdots & \mathbf{T}_{NN} \end{bmatrix}, \tag{37}$$

$$[\mathbf{L}] = \begin{bmatrix} \mathbf{L}_{11} & \mathbf{L}_{12} & \cdots & \mathbf{L}_{1N} \\ \mathbf{L}_{21} & \mathbf{L}_{22} & \cdots & \mathbf{L}_{2N} \\ \vdots & \vdots & \ddots & \vdots \\ \mathbf{L}_{N1} & \mathbf{L}_{N2} & \cdots & \mathbf{L}_{NN} \end{bmatrix}, \tag{38}$$

$$[\mathbf{M}] = \begin{bmatrix} \mathbf{M}_{11} & \mathbf{M}_{12} & \cdots & \mathbf{M}_{1N} \\ \mathbf{M}_{21} & \mathbf{M}_{22} & \cdots & \mathbf{M}_{2N} \\ \vdots & \vdots & \ddots & \vdots \\ \mathbf{M}_{N1} & \mathbf{M}_{N2} & \cdots & \mathbf{M}_{NN} \end{bmatrix}, \tag{39}$$

$$\{\mathbf{w}\} = \begin{Bmatrix} \mathbf{w}_1 \\ \mathbf{w}_2 \\ \vdots \\ \mathbf{w}_N \end{Bmatrix}, \{\mathbf{t}\} = \begin{Bmatrix} \mathbf{t}_1 \\ \mathbf{t}_2 \\ \vdots \\ \mathbf{t}_N \end{Bmatrix}, \tag{40}$$

where the vectors $\{\mathbf{w}_k\}$ and $\{\mathbf{t}_k\}$ are in the forms of $\{a_0^k\ a_1^k\ b_1^k \cdots a_M^k\ b_M^k\}^T$ and $\{p_0^k\ p_1^k\ q_1^k \cdots p_M^k\ q_M^k\}^T$, respectively; the first subscript "j" ($j = 1,2,\ldots,N$) in $[\mathbf{U}_{jk}]$, $[\mathbf{T}_{jk}]$, $[\mathbf{L}_{jk}]$ and $[\mathbf{M}_{jk}]$ denotes the index of the jth ellipse where the collocation point is located and the second subscript "k" ($k = 1,2,\ldots,N$) denotes the index of the kth ellipse where the boundary data $\{\mathbf{w}_k\}$ and $\{\mathbf{t}_k\}$ are specified and M indicates the truncated terms of Fourier series. The coefficient matrix of the linear algebraic system is partitioned into blocks, and each off-diagonal block corresponds to the influence matrices between two different elliptical holes. The diagonal blocks are the influence matrices due to itself in each individual hole. After uniformly collocating the null-field point along the kth elliptical boundary, the submatrix can be written as

$$[\mathbf{K}_{jk}] = \begin{bmatrix} K_{jk}^{0c}(\eta_1) & K_{jk}^{1c}(\eta_1) & K_{jk}^{1s}(\eta_1) & \cdots & K_{jk}^{Mc}(\eta_1) & K_{jk}^{Ms}(\eta_1) \\ K_{jk}^{0c}(\eta_2) & K_{jk}^{1c}(\eta_2) & K_{jk}^{1s}(\eta_2) & \cdots & K_{jk}^{Mc}(\eta_2) & K_{jk}^{Ms}(\eta_2) \\ K_{jk}^{0c}(\eta_3) & K_{jk}^{1c}(\eta_3) & K_{jk}^{1s}(\eta_3) & \cdots & K_{jk}^{Mc}(\eta_3) & K_{jk}^{Ms}(\eta_3) \\ \vdots & \vdots & \vdots & \ddots & \vdots & \vdots \\ K_{jk}^{0c}(\eta_{2L}) & K_{jk}^{1c}(\eta_{2L}) & K_{jk}^{1s}(\eta_{2L}) & \cdots & K_{jk}^{Mc}(\eta_{2L}) & K_{jk}^{Ms}(\eta_{2L}) \\ K_{jk}^{0c}(\eta_{2L+1}) & K_{jk}^{1c}(\eta_{2L+1}) & K_{jk}^{1s}(\eta_{2L+1}) & \cdots & K_{jk}^{Mc}(\eta_{2L+1}) & K_{jk}^{Ms}(\eta_{2L+1}) \end{bmatrix}, \tag{41}$$

where K can be substituted by U, T, L or M. Although the matrix in Eq. (42) is not sparse, it is diagonally dominant. It is found that the influence coefficient for the higher-order harmonics is smaller. It is noted that the superscript "0s" in Eq. (42) disappears since $\sin(0\eta) = 0$. The element of $[\mathbf{K}_{jk}]$ is defined, respectively, as

$$K_{jk}^{nc}(\eta_m) = \int_{B_k} K(\mathbf{s}_k,\mathbf{x}_m) \cos(n\bar{\eta}_k) \bar{\xi}_k d\bar{\eta}_k, \tag{42}$$

$$K_{jk}^{ns}(\eta_m) = \int_{B_k} K(\mathbf{s}_k,\mathbf{x}_m) \sin(n\bar{\eta}_k) \bar{\xi}_k d\bar{\eta}_k, \tag{43}$$

where $n = 0, 1, 2, \ldots, M$, $m = 1, 2, \ldots, 2M + 1$, and η_m is the angle coordinate of the collocating points $\mathbf{x}_m$ along the boundary in the elliptical coordinates. The physical meaning of the influence coefficient for $K_{jk}^{nc}(\eta_m)$ in Eq. (42) denotes the response at $\mathbf{x}_m$ due to $\cos(n\bar{\eta})$ distribution.

3.5. Solution procedures and interface conditions

In the real computation, two problems in Figs. 2b and 3b are solved by using the present formulation. For the exterior problem of the matrix in Fig. 3b, we have

$$[\mathbf{T}^M]\{\mathbf{w}^M - \mathbf{w}^\infty\} - [\mathbf{U}^M]\{\mathbf{t}^M - \mathbf{t}^\infty\} = \{0\}, \tag{44}$$

from Eq. (23). For the interior problem of each inclusion in Fig. 2b, we have

$$[\mathbf{T}^I]\{\mathbf{w}^I\} - [\mathbf{U}^I]\{\mathbf{t}^I\} = \{0\}, \tag{45}$$

from Eq. (19), where the subscripts "M" and "I" denote the matrix and inclusion, respectively. The four influence matrices, $[\mathbf{U}^M]$, $[\mathbf{T}^M]$, $[\mathbf{U}^I]$ and $[\mathbf{T}^I]$, are obtained from the degenerate kernels, while $\{\mathbf{w}^M\}$, $\{\mathbf{t}^M\}$, $\{\mathbf{w}^I\}$, $\{\mathbf{t}^I\}$ represent the coefficient vectors of Fourier series. Based on the continuity of displacement and equilibrium of traction between the interface of matrix and the kth inclusion as shown in Eqs. (6) and (7), we have

$$\{\mathbf{w}^M\} - \{\mathbf{w}^I\} = \{0\}, \tag{46}$$

$$[\boldsymbol{\mu}_0]\{\mathbf{t}^M\} + [\boldsymbol{\mu}_k]\{\mathbf{t}^I\} = \{0\}, \tag{47}$$

where

$$[\boldsymbol{\mu}_0] = \begin{bmatrix} \mu_0 & 0 & \cdots & 0 \\ 0 & \mu_0 & \cdots & 0 \\ \vdots & \vdots & \ddots & \vdots \\ 0 & 0 & \cdots & \mu_0 \end{bmatrix}, [\boldsymbol{\mu}_k] = \begin{bmatrix} \mu_k & 0 & \cdots & 0 \\ 0 & \mu_k & \cdots & 0 \\ \vdots & \vdots & \ddots & \vdots \\ 0 & 0 & \cdots & \mu_k \end{bmatrix}, \tag{48}$$

in which μ_0 and μ_k are the shear moduli of matrix and the kth inclusion, respectively. According to Eqs. (45)–(48), we have a linear system as follows:

$$\begin{bmatrix} \mathbf{T}^M & -\mathbf{U}^M & 0 & 0 \\ 0 & 0 & \mathbf{T}^I & -\mathbf{U}^I \\ \mathbf{I} & \mathbf{0} & -\mathbf{I} & 0 \\ 0 & \boldsymbol{\mu}_0 & 0 & \boldsymbol{\mu}_k \end{bmatrix} \begin{Bmatrix} \mathbf{w}^M \\ \mathbf{t}^M \\ \mathbf{w}^I \\ \mathbf{t}^I \end{Bmatrix} = \begin{Bmatrix} \mathbf{c} \\ 0 \\ 0 \\ 0 \end{Bmatrix}, \tag{49}$$

where $[\mathbf{I}]$ is the identity matrix and $\{\mathbf{c}\}$ is the forcing term due to the remote shear stress as shown below

$$\{\mathbf{c}\} = [\mathbf{T}^M]\{\mathbf{w}^\infty\} - [\mathbf{U}^M]\{\mathbf{t}^\infty\}. \tag{50}$$

From Eq. (49), the unknown Fourier coefficients can be easily determined.

4. Illustrative examples and discussions

4.1. Example 1: an infinite plane with an elliptical hole or an elliptical rigid inclusion

The sketch shown in Fig. 6 is an infinite plane with an elliptical hole under the remote shear. For this case, the analytical solution of Smith [27] was obtained to verify the validity of our approach. He obtained the solution of a circular case first. Then, the ellipse in the z plane is mapped into the unit circle $|\zeta| = R_0$ in the ζ plane by using the conformal mapping as follows:

$$\zeta = \frac{R_0}{a+b}\left[z + (z^2 + c^2)^{1/2}\right]. \tag{51}$$

For the Neumann case without considering the dislocation, the anti-displacement field can be described by

$$w = \mathrm{Re}\left\{\frac{a+b}{2R_0}(\tau_{xz} - i\tau_{yz})\zeta + \frac{a+b}{2R_0}(\tau_{xz} + i\tau_{yz})\frac{R_0^2}{\zeta}\right\}, \tag{52}$$

where Re{·} denotes the real part. We also consider the Dirichlet-type case and the solution is represented by

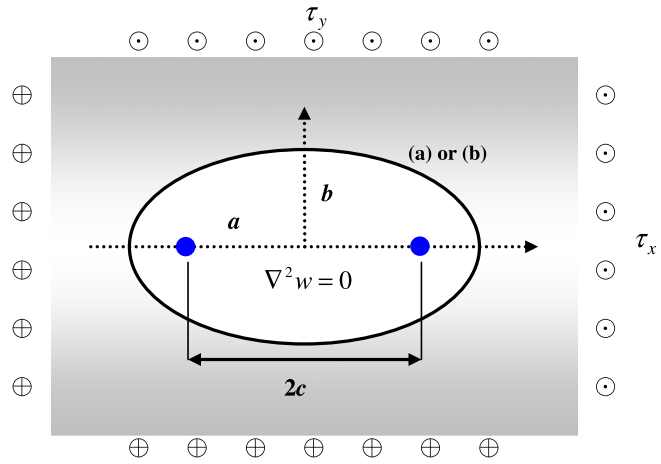

Fig. 6. An infinite plane with an elliptic inclusion under remote shears (boundary conditions: (a) a hole ($w = 0$) and (b) a rigid inclusion ($\frac{\partial w}{\partial n} = 0$).

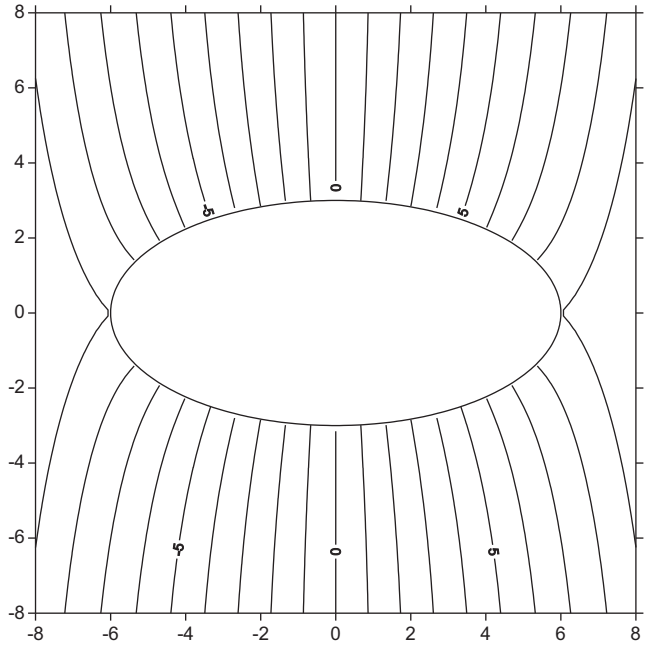

Fig. 7a. Contour plot of Smith's solution (Neumann B.C.).

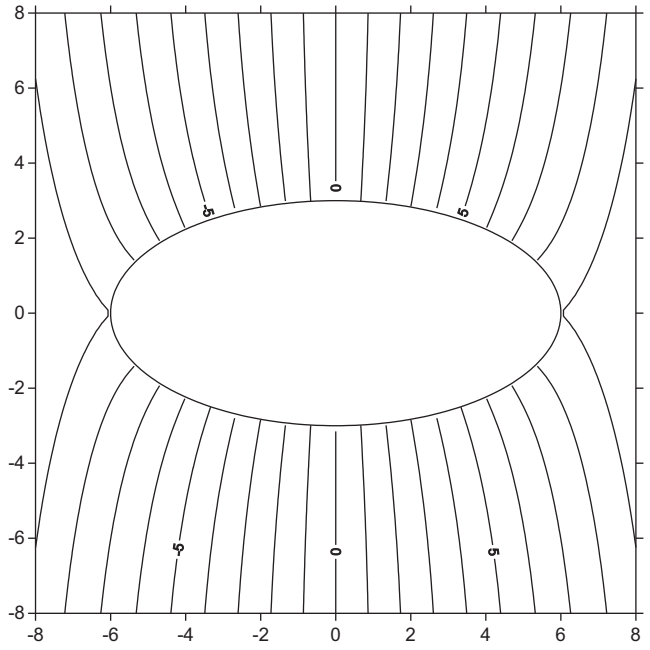

Fig. 7b. Contour plot of the present approach (Neumann B.C.).

$$w = \mathrm{Re}\left\{\frac{a+b}{2R_0}(\tau_{xz} - i\tau_{yz})\zeta - \frac{a+b}{2R_0}(\tau_{xz} + i\tau_{yz})\frac{R_0^2}{\zeta}\right\}. \tag{53}$$

Now, the problem is revisited by using the present approach. Here, we consider the Neumann boundary condition ($\frac{\partial w}{\partial n} = 0$) on the hole first. As mentioned in Section 2, the problem can be decomposed into two parts. One is the remote shear in an infinite plane and another is the infinite plane problem with an elliptical hole. Since

$$\frac{\partial w}{\partial n} = \frac{\partial w^\infty}{\partial n} + \frac{\partial \bar{w}}{\partial n} = 0, \tag{54}$$

the boundary condition of elliptic cylinder in an infinite plane is

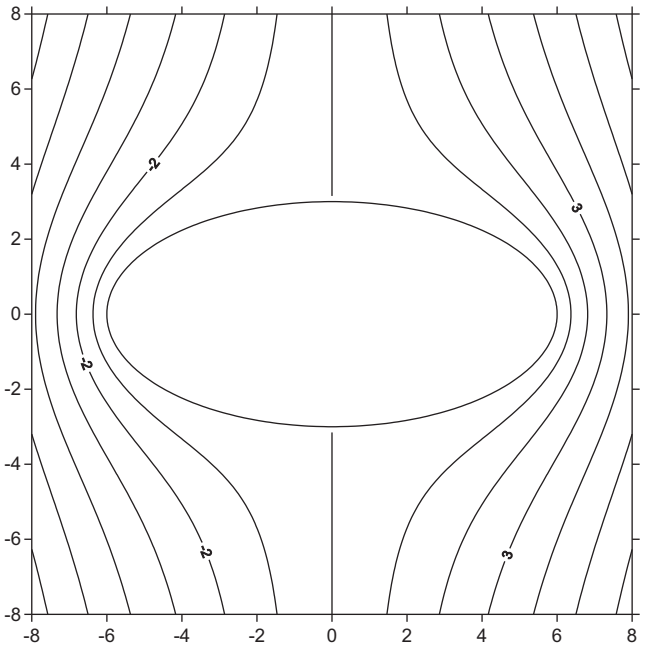

Fig. 8a. Contour plot of Smith's solution (Dirichlet B.C.).

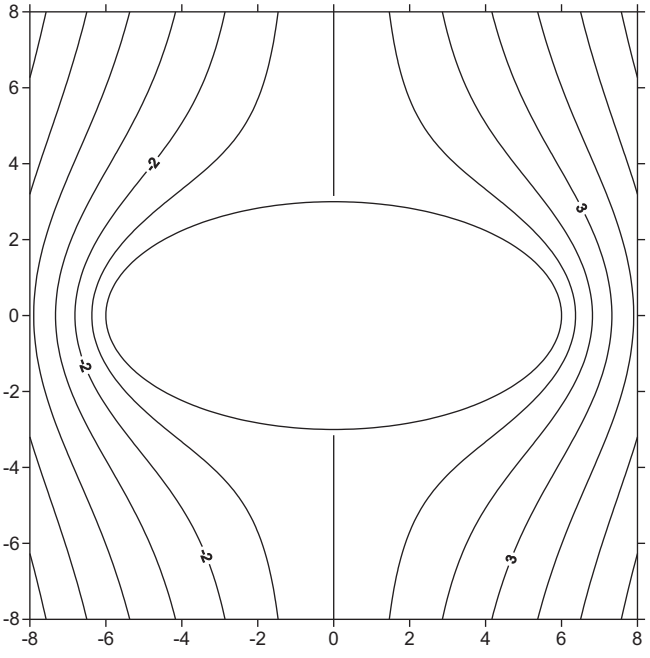

Fig. 8b. Contour plot of the present approach (Dirichlet B.C.).

$$\frac{\partial \bar{w}}{\partial n} = -\frac{\partial w^{\infty}}{\partial n} = \frac{\tau_{xz}}{\mu} n_x + \frac{\tau_{yz}}{\mu} n_y = \frac{c}{J}\left(\frac{\tau_{xz}}{\mu}\sinh\bar{\xi}\cos\bar{\eta} + \frac{\tau_{yz}}{\mu}\cosh\bar{\xi}\sin\bar{\eta}\right). \quad (55)$$

By comparing with Eq. (30), the Fourier coefficients are obtained as

$$p_1 = c\frac{\tau_{xz}}{\mu}\sinh\bar{\xi}, \quad q_1 = c\frac{\tau_{yz}}{\mu}\cosh\bar{\xi}, \quad p_n = q_n = 0, \quad n \neq 1. \quad (56)$$

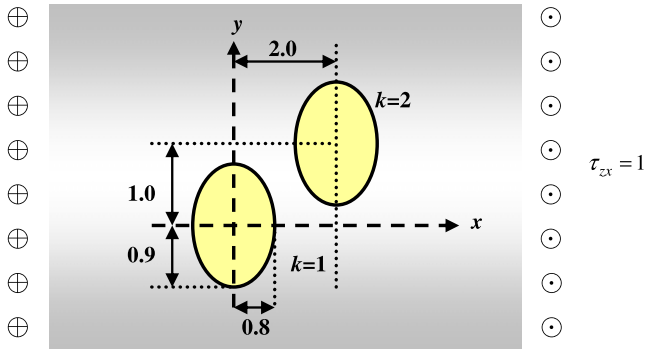

Fig. 9a. Case A: An infinite plane with two elliptical inclusions under a remote shear at x axis ($\tau_{xz} = 1$).

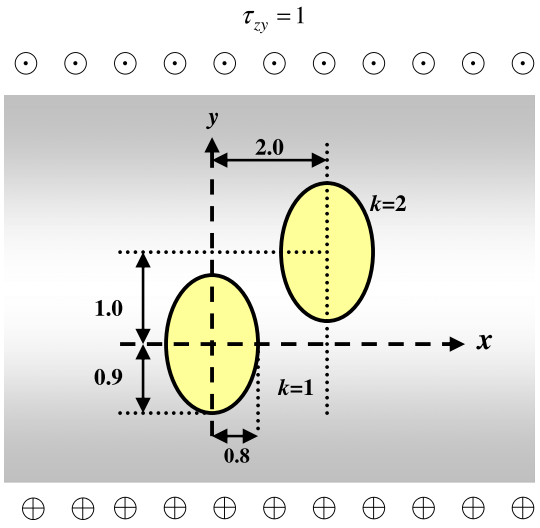

Fig. 9b. Case B: An infinite plane with two elliptical inclusions under a remote shear at y axis ($\tau_{yz} = 1$).

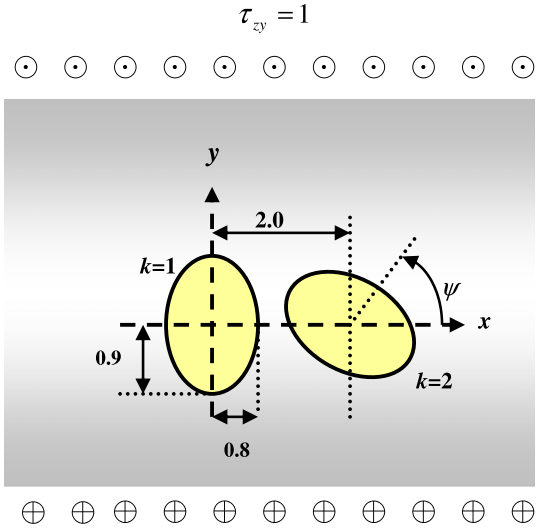

Fig. 9c. Case C: An infinite plane with two elliptical inclusions subject to an inclination angle under a remote shear ($\tau_{yz} = 1$, one slant inclusion).

After using the null-field integral equation in Eq. (23), the unknown Fourier coefficients are obtained as

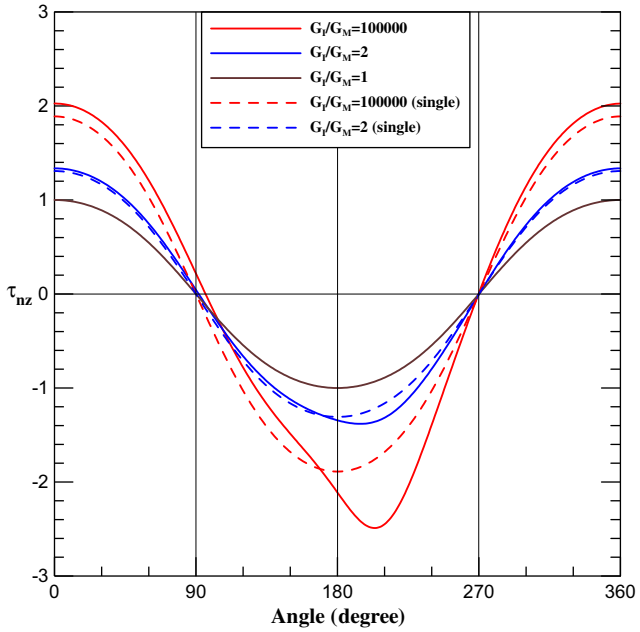

Fig. 10a. Normal stress distribution of case A (the present approach).

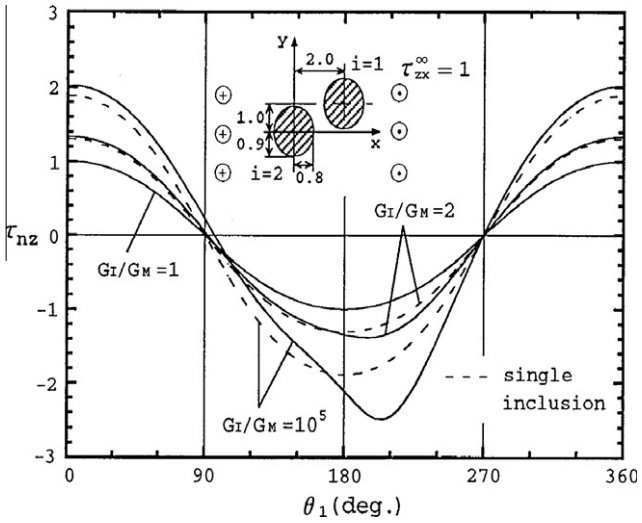

Fig. 10b. Normal stress distribution of case A by Noda and Matsuo [21].

$$a_0 = \textit{arbitrary},$$
$$a_1 = p_1 = \frac{\tau_{xz}}{\mu} c \sinh\bar{\xi},$$
$$b_1 = q_1 = \frac{\tau_{yz}}{\mu} c \cosh\bar{\xi}. \tag{57}$$

For simplicity, we choose $a_0 = 0$. After obtaining unknown Fourier coefficients and given boundary conditions, we have the second-part solution

$$\bar{w}(\xi,\eta) = \frac{\tau_{xz}}{\mu} e^{-\xi} c \sinh\bar{\xi}(\cosh\bar{\xi} + \sinh\bar{\xi}) \cos\eta + \frac{\tau_{yz}}{\mu} e^{-\xi} c \times \cosh\bar{\xi}(\cosh\bar{\xi} + \sinh\bar{\xi}) \sin\eta, \tag{58}$$

where $\bar{\xi} = \tanh^{-1}(b/a)$. Then, the total field can be obtained by superimposing the two parts as follows:

$$w = w^{\infty} + \bar{w} = \frac{\tau_{xz}}{\mu} c \cosh\xi \cos\eta + \frac{\tau_{yz}}{\mu} c \sinh\xi \sin\eta + \frac{\tau_{xz}}{\mu} e^{-\xi} c \times \sinh\bar{\xi}(\cosh\bar{\xi} + \sinh\bar{\xi}) \cos\eta + \frac{\tau_{yz}}{\mu} e^{-\xi} c \cosh\bar{\xi}(\cosh\bar{\xi} + \sinh\bar{\xi}) \sin\eta. \tag{59}$$

Fig. 7a is the contour plot by using Smith's solution in Eq. (52) and considered $\tau_{xz} = 0$ and $\tau_{yz} = 1$ after rotating 90° in a clockwise way. Fig. 7b shows the contour plot for case of $\tau_{xz} = 1$ and $\tau_{yz} = 0$ by using the present approach. After comparing the two figures, it is observed that our result matches well with the Smith's solution. Another rigid inclusion case (Dirichlet-type boundary condition) is also utilized to verify the validity of the present approach. In a similar way, we have the second-part field solution

$$\bar{w}(\xi,\eta) = -\frac{\tau_{xz}}{\mu} e^{-\xi} c \cosh\bar{\xi}(\cosh\bar{\xi} + \sinh\bar{\xi}) \cos\eta - \frac{\tau_{yz}}{\mu} e^{-\xi} c \times \sinh\bar{\xi}(\cosh\bar{\xi} + \sinh\bar{\xi}) \sin\eta. \tag{60}$$

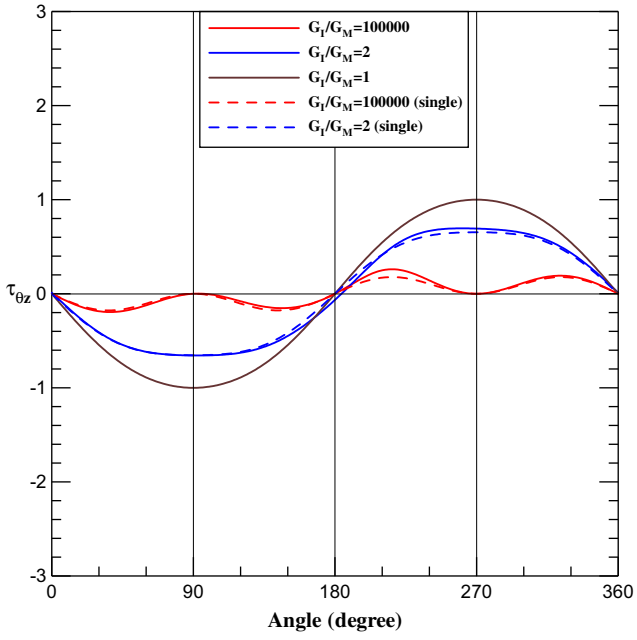

Fig. 11a. Tangential stress distribution of case B (the present approach).

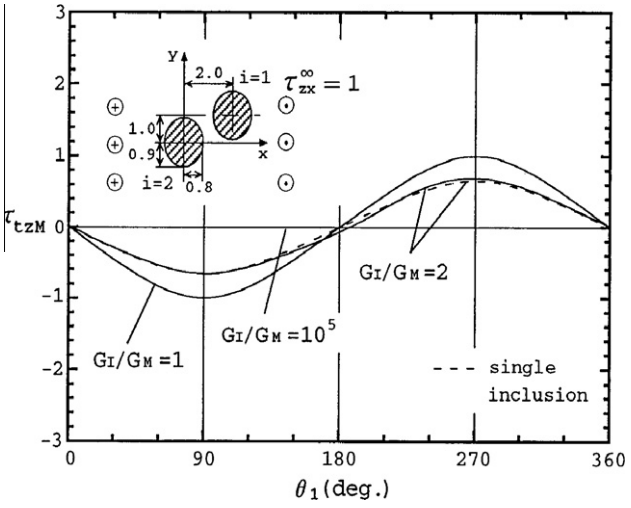

Fig. 11b. Tangential stress distribution of case B by Noda and Matsuo [21].

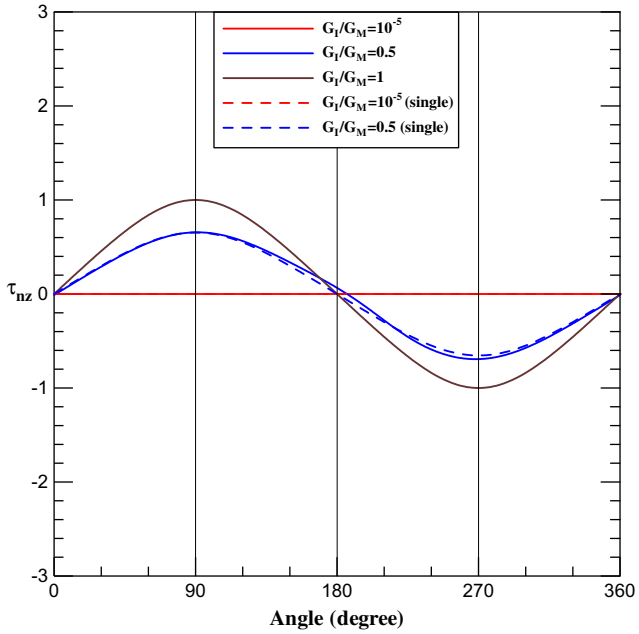

Fig. 12a. Normal stress distribution of case B (the present approach).

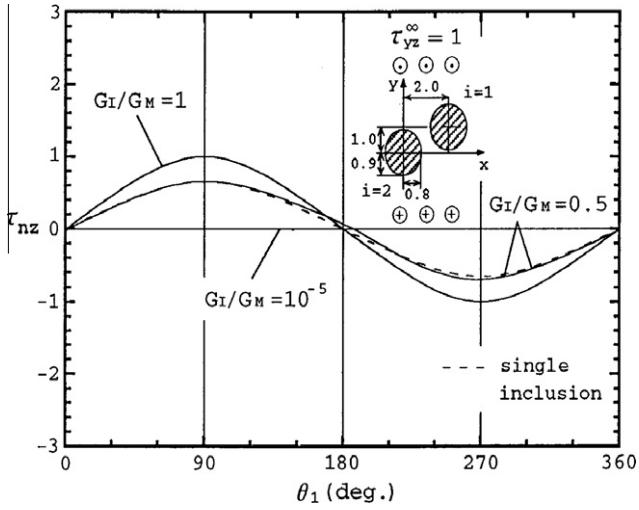

Fig. 12b. Normal stress distribution of case B by Noda and Matsuo [21].

Then, the total field can be obtained by superimposing the two parts as follows:

$$w = w^{\infty} + \bar{w} = \frac{\tau_{xz}}{\mu} c \cosh\xi \cos\eta + \frac{\tau_{yz}}{\mu} c \sinh\xi \sin\eta - \frac{\tau_{xz}}{\mu} e^{-\xi} c \times \cosh\bar{\xi}(\cosh\bar{\xi} + \sinh\bar{\xi}) \cos\eta - \frac{\tau_{yz}}{\mu} e^{-\xi} c \sinh\bar{\xi}(\cosh\bar{\xi} + \sinh\bar{\xi}) \sin\eta. \quad (61)$$

Similarly, Fig. 8a shows the contour plot by using Smith's solution [27] in Eq. (53) and considered $\tau_{xz} = 0$ and $\tau_{yz} = 1$ after rotating 90° in a clockwise way. Fig. 8b shows the contour plot for case of $\tau_{xz} = 1$ and $\tau_{yz} = 0$ by using the present approach. Although the solution forms between ours and Smith's look different, good agreements from contour plots not only in the Neumann problem but also in the Dirichlet problem are made in real calculations.

4.2. Example 2: an infinite plane with two elliptical inclusions

The interaction problem of two identical elliptical inclusions in an infinite plane with remote shears is considered. The shear moduli of two inclusions are the same ($\mu_1 = \mu_2$). In this example, three cases of different locations of two inclusions are considered in the demonstrative examples as shown in Figs. 9a–9c. These cases have been solved by Noda and Matsuo [21] by using the singular integral equation method. Lee and Kim [22] also revisited cases A and B for the modulus ratios of 0.5, and 2.0 to verify their solutions of the volume integral equation method. Besides, they also provided the results for modulus ratios of 0.25 and 4. For the case A as shown in Fig. 9a, the normal stresses on the matrix surface of the second inclusion with respective to different ratio of shear moduli ($\mu_2/\mu_0 = 1$, 2 and 10^5) are shown in Fig. 10a. Also, the single-inclusion case ($\mu_1 = \mu_0$) is considered by using the present approach. After comparing with the results of Noda and Matsuo as shown in Fig. 10b, good agreements are made. Fig. 11a shows the tangential stresses on the matrix surface of the second inclusion. After comparing with the results of Noda and Matsuo shown in Fig. 11b, we found that our result deviates from Noda and Matsuo's data when the ratio of shear moduli ($\mu_2/\mu_0 = 10^5$) is considered. However, our results compare well with those of Noda and Matsuo for the other ratio of shear moduli ($\mu_2/\mu_0 = 1$, 2). When the case $\mu_2/\mu_0 = 1$ is considered, it can be seen as a special case of an infinite plane without any holes or inclusions. Regarding the deviation between the result of Noda and Matsuo and ours for the modulus ratio of 10^5, the issue is open for discussion. For the case B as shown in Figs. 9b, 12a and 13a show the normal stresses and tangential stress, respectively, on the matrix surface of the second inclusion with respective to different ratio of shear moduli ($\mu_2/\mu_0 = 1$, 0.5 and 10^{-5}). A single-inclusion case ($\mu_1 = \mu_0$) was also taken into consideration. After comparing with the results of Noda and Matsuo as shown in Figs. 12b and 13b, good agreements are made. When the case $\mu_2/\mu_0 = 10^{-5}$ is considered, it can be seen as a special case of an infinite plane containing two holes. The last case as shown in Fig. 9c is two identical inclusions and located on the x-axis with different orientation. Fig. 14a shows the normal stresses on matrix surface of the second inclusion with respective

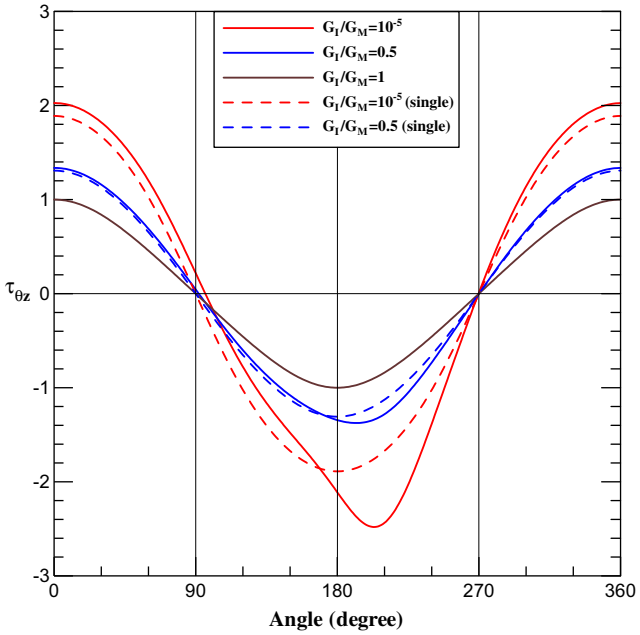

Fig. 13a. Tangential stress distribution of case B (the present approach).

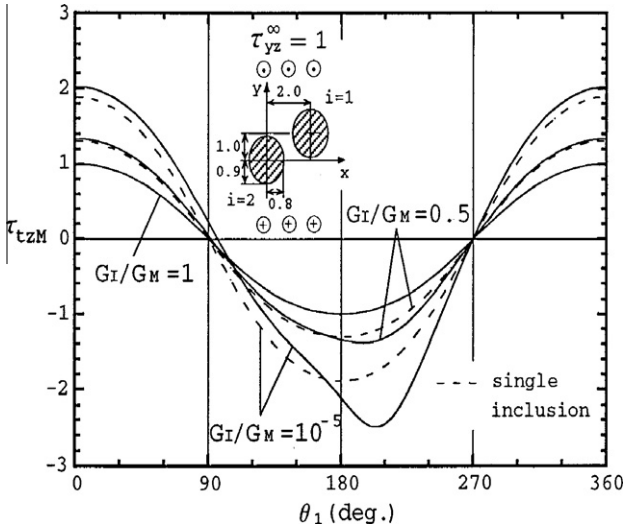

Fig. 13b. Tangential stress distribution of case B by Noda and Matsuo [21].

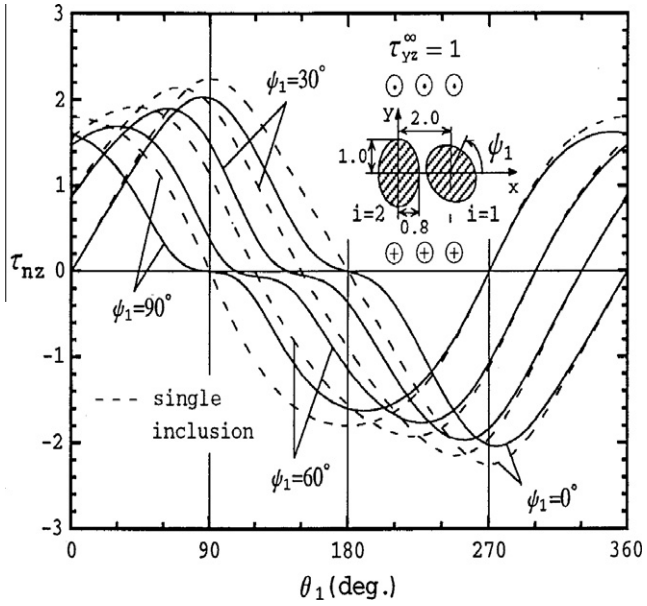

Fig. 14b. Tangential stress distribution of case C by Noda and Matsuo [21].

to different inclination angle (ψ = 0°, 30°, 60° and 90°). The results of single-inclusion ($\mu_1 = \mu_0$) are also shown in Fig. 14a. It is found that our results are consistent with those of Noda and Matsuo after comparing with Fig. 14b. Besides, we also found the description of the inclusion size in the figure sketch is not consistency with the figure caption in the paper of Noda and Matsuo [21]. Here, we adopt the size description in the figure caption and compare our results well.

In the all cases, the elliptical inclusions are not very oblate. When elliptical inclusions become more oblate, the stress field has a larger varying gradient near elliptical inclusions. The present work is implemented by using the elliptical coordinates. When an elliptical inclusion becomes more oblate, there is no difficulty for the present approach. However, a larger number of truncation terms of eigenfunction for more oblate case may be taken in the semi-analytical approach.

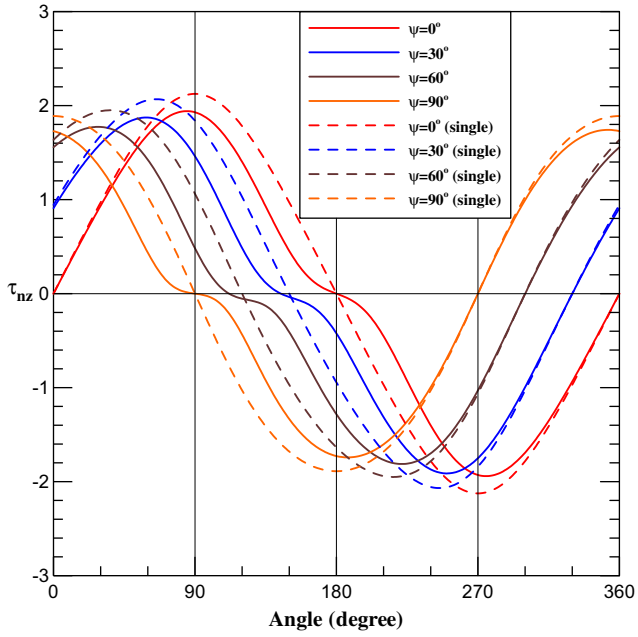

Fig. 14a. Normal stress distribution of case C (the present approach).

5. Concluding remarks

We have successfully proposed a systematic method by using the null-field integral formulation in conjunction with degenerate kernels and eigenfunction expansion for solving the infinite plane with elliptical holes and/or inclusions under remote shear. The fundamental solution was expanded to a degenerate kernel by using the elliptical coordinates. Although Jacobian term may appear in the degenerate kernel, boundary density and boundary contour integral by using the elliptical coordinates, it can be cancelled out in our formulation to preserve the orthogonal condition. Free of calculating principal value of using the small circular bump method is our advantage over the conventional boundary integral equation. After employing the collocation method, the linear algebraic equation can be established and the Fourier coefficients are easily determined although the addition theorems are mostly mentioned when they are used to analytically set up the system of equations. Besides, our series solutions for the antiplane problem are found to agree with the closed-form solution of Smith. The present approach can be seen as an alternative, natural and logical method to solve antiplane problems with elliptical boundaries. Besides, its extension to three dimensional problems may be possible if the degenerate kernel is available. Finally, a general program is developed for the antiplane problem with elliptical inclusions of arbitrary number, position, size and inclination angle. Good agreement is made after comparing with those in the literature.

Acknowledgement

Financial support from the National Science Council under Grant No. NSC-100-2811-E-019-001 for National Taiwan Ocean University is gratefully acknowledged.

References

[1] Goree JG, Wilson HB. Transverse shear loading in an elastic matrix containing two circular cylindrical inclusions. ASME J Appl Mech 1967;34:511–3.
[2] Budiansky B, Carrier GF. High shear stresses in stiff-fiber composites. ASME J Appl Mech 1984;51:733–5.
[3] Steif PS. Shear stress concentration between holes. ASME J Appl Mech 1989;56:719–21.

[4] Zimmerman RW. Second-order approximation for the compression of an elastic plate containing a pair of circular holes. Z Angew Math Mech 1998;68:575–7.
[5] Gong SX. Antiplane interaction among multiple circular inclusions. Mech Res Commun 1995;22(3):257–62.
[6] Chao CK, Young CW. On the general treatment of multiple inclusions in antiplane elastostatics. Int J Solids Struct 1998;35:3573–93.
[7] Wu LZ. Interaction of two circular cylindrical inhomogeneities under anti-plane shear. Compos Sci Technol 2000;60:2609–15.
[8] Steif PS. Longitudinal shearing of a weakly bonded fiber composite. ASME J Appl Mech 1998;55:618–23.
[9] Sendeckyj GP. Multiple circular inclusion problems in longitudinal shear deformation. J Elast 1971;1(1):83–6.
[10] Honein E, Honein T, Herrmann G. On two circular inclusions in harmonic problems. Q Appl Math 1992;50:479–99.
[11] Chen JT, Chou KH, Lee YT. A novel method for solving the displacement and stress fields of an infinite domain with circular holes and/or inclusions. Acta Mech 2011;218:115–32.
[12] Chou SI. Stress field around holes in antiplane shear using complex variable boundary element method. ASME J Appl Mech 1997;64:432–5.
[13] Mogilevskaya SG, Crouch SL. A Galerkin boundary integral method for multiple circular elastic inclusions. Int J Numer Methods Eng 2001;52:1069–106.
[14] Chen JT, Shen WC, Wu AC. Null-field integral equations for stress field around circular holes under antiplane shear. Eng Anal Bound Elem 2006;30:205–17.
[15] Chen JT, Wu AC. Null-field approach for the multi-inclusion problem under anti-plane shears. ASME J Appl Mech 2007;74:469–87.
[16] Chen JT, Wu AC. Null-field approach for piezoelectricity problems with arbitrary circular inclusions. Eng Anal Bound Elem 2006;30:971–93.
[17] Gong SX, Meguid SA. A general treatment of the elastic field of an elliptical inhomogeneity under antiplane shear. ASME J Appl Mech 1992;59:131–5.
[18] Gong SX. A unified treatment of the elastic elliptical inhomogeneity under antiplane shear. Arch Appl Mech 1995;65:55–64.
[19] Ru CQ, Schiavone P. On the elliptic inclusion in anti-plane shear. Math Mech Solids 1996;1:327–33.
[20] Shen H, Schiavone P, Ru CQ, Mioduchowski A. An elliptic inclusion with imperfect interface in anti-plane shear. Int J Solids Struct 2000;37:4557–75.
[21] Noda NA, Matsuo T. Stress analysis of arbitrarily distributed elliptical inclusions under longitudinal shear loading. Int J Fract 2000;106:81–93.
[22] Lee J, Kim HR. Volume integral equation method for multiple circular and elliptical inclusion problems in antiplane elastostatics. Composites-B 2012;43:1224–43.
[23] Ting K, Chen KT, Yang WS. Boundary element alternating method applied to analyze the stress concentration problems of multiple elliptical holes in an infinite domain. Nucl Eng Des 1999;187(3):303–13.
[24] Kushch VI, Shmegera SV, Buryachenko VA. Interacting elliptic inclusions by the method of complex potentials. Int J Solids Struct 2005;42:5491–512.
[25] Kushch VI, Shmegera SV, Buryachenko VA. Elastic equilibrium of a half plane containing a finite array of elliptic inclusions. Int J Solids Struct 2006;43:3459–83.
[26] Kuo H-Y. Electrostatic interactions of arbitrarily dispersed multicoated elliptic cylinders. Int J Eng Sci 2010;48:370–82.
[27] Smith E. The interaction between dislocations and inhomogeneities – I. Int J Eng Sci 1968;6:129–43.
[28] Kane JH. Boundary element analysis in engineering continuum mechanics. NJ: Prentice Hall; 1994.
[29] Banerjee PK, Butterfield R. Boundary element methods in engineering science. London: McGraw-Hill; 1981.
[30] Wrobel LC. The boundary element method. New York: John Wiley; 2002.
[31] Kellogg OD. Foundations of potential theory. Dover Publications; 1969.
[32] Mikhlin SG. Mathematical physics: an advanced course. Amsterdam: North-Holland Publishing Company; 1970.